against the particle volume fraction ϕ for Gz of 10 and 15 increases sharply up to volume fraction of 5% beyond which the increase is very slow. For a Gz of 15 and a suspension of volume fraction of 5% the overall heat transfer coefficient is 1.6 times that for the aqueous NaCl.

The ratio of Nusselt number of flowing suspensions, Nu_s, to that of aqueous NaCl, Nu, is plotted against the particle volume fraction ϕ in Fig. 4. It increases linearly with ϕ sharply up to 5% beyond which the increase is very slow. Number of heat transfer units, NTU, is plotted against ϕ with Gz as parameter in Fig. 5(a). At a given Gz, greater particle volume fractions yield larger values of NTU which means, as is apparent in equation (6), larger values of heat exchanger effectiveness. This conclusion is shown more clearly in Fig. 5(b).

Augmentation values of Nusselt number from Fig. 4 and of heat exchanger effectiveness from Fig. 5(b) both at Gz of 15, are included in Table 1. By employing the values of the properties assembled elsewhere [2], the increases in power expenditure for propelling suspensions (computed from equation (5)) are also included in Table 1. It is seen that the Nusselt number and the heat exchanger effectiveness are enhanced significantly while the increase in the power expenditure is much lower.

SUMMARY

By a series of experiments, the existence of augmentation of heat transfer in laminar flow of particle suspensions has been demonstrated. The origin of this augmentation resides in the shear induced particle rotations and the concomitant churning of the embedding fluid. Effects of particle diameter and volume fraction, tube dimensions, suspending fluid diffusivities and shear rate on heat transfer have been explored and found to be appreciable. The heat transfer data have been presented for the purpose of the thermal design of a heat exchanger. Relative to heat transfer in pure suspending liquid, Nusselt number is augmented by 82% for a 100 μm dia. particle suspension of volume fraction of 4.64% at Graetz number of 15. The heat exchanger effectiveness is enhanced by 25%, while the energy expenditure for propelling the suspension is increased by only 8%.

REFERENCES

1. A. S. Ahuja, Heat transport in laminar flow of erythrocyte suspensions, *J. appl. Physiol.* **39**, 86–92 (1975).
2. A. S. Ahuja, Augmentation of heat transport in laminar flow of polystyrene suspensions. I. Experiments and results, *J. appl. Phys.* **46**, 3408–3416 (1975).
3. A. S. Ahuja, Augmentation of heat transport in laminar flow of polystyrene suspensions. II. Analysis of the data, *J. appl. Phys.* **46**, 3417–3425 (1975).
4. A. S. Ahuja, Augmentation of heat and mass transport in flowing particle suspensions: A dimensional analysis. *J. appl. Phys.* **47**, 775–777 (1976).
5. A. S. Ahuja, W. R. Hendee and P. L. Carson, Transport phenomena in laminar flow of blood, *Phys. Med. Biol.* **23**, 928–936 (1978).
6. A. S. Ahuja, Augmentation of heat and mass transfer in laminar flow of suspensions: A correlation of data, *J. appl. Phys.* **51**, 791–795 (1980).
7. A. S. Ahuja and W. R. Hendee, Thermal design of a heat exchanger for heating or cooling blood, *Phys. Med. Biol.* **23**, 937–951 (1978).
8. A. E. Bergles, Survey and evaluation of techniques to augment convective heat and mass transfer, in *Progress in Heat and Mass Transfer* (Edited by U. Grigull and E. Hahne). Vol. 1, pp. 331–424. Pergamon Press, New York (1969).
9. A. E. Bergles and R. L. Webb (eds.), *Augmentation of Convective Heat and Mass Transfer*. ASME, New York (1970).
10. A. E. Bergles, Recent developments in convective heat-transfer augmentation, *Appl. Mech. Rev.* **26**, 675 (1973).
11. A. S. Ahuja, Measurement of thermal conductivity of (neutrally and nonneutrally buoyant) stationary suspensions by the unsteady-state method, *J. appl. Phys.* **46**, 747–755 (1975).
12. E. R. G. Eckert and R. M. Drake, Jr., *Heat and Mass Transfer*, 2nd edn. McGraw-Hill, New York (1959).

Int. J. Heat Mass Transfer. Vol. 25, No. 5, pp. 728–736, 1982
Printed in Great Britain
0017-9310/82/050728-09 $03.00/0

RADIATION CONFIGURATION FACTORS FOR OBLIQUELY ORIENTED FINITE LENGTH CIRCULAR CYLINDERS

ALIASGHAR AMERI and JAMES D. FELSKE

Department of Mechanical and Aerospace Engineering, State University of New York at Buffalo, Amherst, NY 14260, U.S.A.

(*Received* 17 *July* 1981 *and in revised form* 21 *September* 1981)

NOMENCLATURE

C, center-to-center spacing of cylinders in the parallel orientation [m];
F, configuration factor;
L, length of cylinder [m];
R, cylinder radius [m].

Greek symbols

θ, ϕ, cylinder rotations defined in Fig. 1 [deg].

Subscripts

max, pertaining to the maximum value of the configuration factor for a ninety degree orientation;
0, parallel orientation, finite length cylinders;
0_∞, parallel orientation, infinitely long cylinders;
θ, cylinder rotation in the theta direction;
ϕ, cylinder rotation in the phi direction.

Superscript

$'$, end-point rotation.

INTRODUCTION

ANALYSES of the diffuse radiative transport between cylinders have so far considered parallel-oriented tubes of either finite [1–3] or infinite lengths [4]. Although general numerical codes have been developed which are capable of computing configuration factors for arbitrarily oriented cylinders [5, 6], such computations have not yet been presented. The purpose of the present study is to develop closed-form approximate expressions for such configuration factors based upon the numerical results obtained by applying a general computer program [6] to this category of problems. The analytical expressions so obtained provide fairly accurate estimates for the configuration factors for this complex geometry. For most engineering design computations, the equations may be used directly. In addition, they provide a means of inexpensively investigating the effects of various design parameters in preliminary studies wherein the greater precision of the numerical computation would be reserved for the final calculations.

NUMERICAL PROCEDURE

In the CONSHAD program [6] the method of contour integration [7, 8] is employed to transform the inner surface area integral into a line integral around its boundary. The formulation given in [7] was followed. The program is capable of computing configuration factors between planar, convex and polygonal surfaces. As such, we have modelled cylinders as polygons of the same surface area. For surfaces which see one another, contour integrals are performed around the boundaries of each polygon which comprises one of the "cylinders". This type of integration is made for each of the surface area elements on the other polygonally-modelled cylinder. The surface area elements are taken to be triangular in shape so as to allow a straightforward subdivision of polygonal surfaces.

The number of sides and subdivisions of a side required to accurately predict cylindrical surface behavior was determined from various tests including comparisons to results for finite and infinitely long parallel cylinders of different spacings [2, 4]. Polygons ranging from 6 to 16 sides were investigated and the number of triangular elements was varied from 144 to 576. It was found that by using a 12-sided polygonal model in which the cylinder for the surface area integration was divided into 144 triangular subsurfaces, that agreement to the third significant figure was achieved for "infinite", parallel cylinders (length/radius = 600 and spacing/radius = 6). Excellent agreement was also achieved between the present computations and the figures presented in [2] for all lengths and spacings of finite length cylinders.

Computations for obliquely oriented cylinders of equal diameter were performed for the basic categories of orientations shown in Fig. 1. These orientations are defined by the indicated θ and ϕ rotations. Results for pure θ-rotations ($\phi = 0°$) were considered for two separate cases in which the cylinders were of the same length and either: (i) one of the cylinders was given a θ-rotation about its mid-point [Fig. 1(b)], or (ii) one of the cylinders was given a θ-rotation about its end-point [Fig. 1(c)]. Results for pure ϕ-rotations ($\theta = 0°$) were computed for half-length to whole-length cylinders [Fig. 1(d)]. Finally, combined θ and ϕ-rotations were considered for half-to whole-length cylinders [Fig. 1(e)] using the convention that the ϕ-rotation was always performed first. For all cases, the configuration factor may be written functionally as:

$$F = F(L/R, C/R, \theta, \phi) \quad (1)$$

where L and R are the length and radius of a cylinder respectively, C is the center-to-center spacing of the cylinders in the parallel orientation, and θ and ϕ are the angular rotations of one cylinder with respect to the other.

θ-ROTATIONS

Mid-point rotation—Fig. 1(b)

For pure θ-rotations ($\phi = 0°$) about the mid-point of one of the cylinders, the configuration factors are symmetric with respect to $\theta = 90°$. Computations were therefore performed for $0 \le \theta \le 90°$. Figure 2 shows a typical variation of the

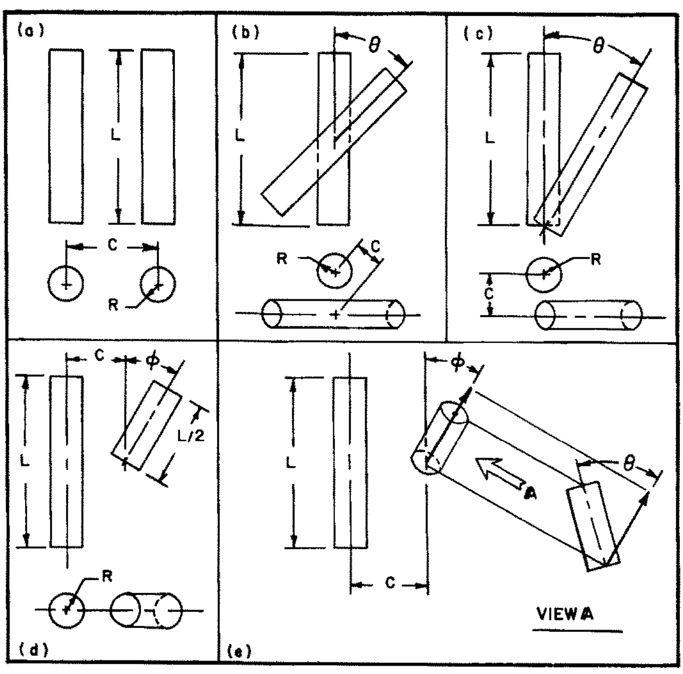

FIG. 1. Cylinder orientations: (a) parallel orientation, (b) mid-point θ-rotation, (c) end-point θ-rotation, (d) ϕ-rotation, (e) combined θ and ϕ rotation (ϕ-rotation first).

configuration factor as a function of θ for four different spacings at a given length to radius ratio. The points computed by numerical integration are denoted by the symbols. The solid lines are the curves defined by the following equation which was found by trial and error to represent the θ variation rather well [8]:

$$\frac{F_\theta}{F_0} = \left(\frac{F_{\theta=90}}{F_0}\right)^{\sin\theta}. \tag{2}$$

The quantity F_0 is the configuration factor for the finite length cylinders in the parallel orientation [$\theta = 0°$, Fig. 1(a)]. This equation gives the exact result for $\theta = 0$ and 90°. The largest differences between the computed points and the analytical representation occur at smaller spacings where F_0 and $F_{\theta=90}$ differ the most. For the cases shown in Fig. 2 a maximum difference of 6.4% occurs at $\theta = 45°$ for $L/R = 37.7$ and $C/R = 3$.

In order to achieve a purely analytical expression for F_θ, simple approximate equations must be developed for F_0 and $F_{\theta=90}$. Such an expression for F_0 has previously been developed by Glicksman [3] based upon physical arguments. This equation is also given in [9] and the full derivation appears in [10]. The result for cylinders of equal diameter is

$$\frac{F_0}{F_{0\infty}} = 1 - \frac{1}{\pi}\left\{\left|\cos^{-1}\left(\frac{B}{A}\right)\right| - \frac{1}{2(L/R)} \times \left[\sqrt{[(4+2)^2 + (2C'/R)^2]} \left|\cos^{-1}\left(\frac{BR}{AC'}\right)\right| + B\left|\sin^{-1}\left(\frac{R}{C'}\right)\right| - \frac{\pi}{2}A\right]\right\} \tag{3}$$

where

$$A = (L/R)^2 + (C'/R)^2 - 1, \tag{4}$$

$$B = (L/R)^2 - (C'/R)^2 + 1, \tag{5}$$

$$C' = C - 0.85R. \tag{6}$$

The quantity $F_{0\infty}$ is the configuration factor for two infinitely long cylinders of parallel orientation. Using the cross-string method for cylinders of equal diameter, it may be written as [4]:

$$F_{0\infty} = \frac{1}{\pi}\left\{\sin^{-1}\left(\frac{2R}{C}\right) + \left[\left(\frac{C}{2R}\right)^2 - 1\right]^{1/2} - \frac{C}{2R}\right\}. \tag{7}$$

A comparison between the configuration factors predicted by equation (3) and those determined by numerical integration show that an average agreement of 1.5% is attained for the range of cylinder lengths and spacings investigated: $0.1 \le L/R \le 1000$ and $3 \le C/R \le 50$. A maximum discrepancy of 3.2% was found for $L/R = 0.1$ with $C/R = 50$. Consequently, Glicksman's result was incorporated into the present approximation.

In attempting to correlate $F_{\theta=90}$, several simple functional forms were initially considered [9]. However, these met with only limited success. In the present study, the function $F_{\theta=90} = F(L/R, C/R, \theta = 90°, \phi = 0°)$ was investigated more fully. Its behavior is shown in Fig. 3. (The characteristic of $F_{\theta=90}$ to achieve a maximum follows from the fact that as either the cylinder length becomes infinitesimally small or infinitely large the configuration factor must approach zero for all spacings.) A universal scaling of these similar looking curves was then sought. The maximum shape factor at a given spacing, $(F_{\theta=90})_{max}$, and the cylinder length at which $(F_{\theta=90})_{max}$ is achieved, $(L/R)_{max}$, were used as the scale factors. From the points plotted in Fig. 4 it is seen that the results of Fig. 3 are well correlated through these scaling factors. The points in Fig. 4 were then represented by the following probability distribution curve which appears as the solid line in the figure:

$$\frac{F_{\theta=90}}{(F_{\theta=90})_{max}} = \left(\frac{(L/R)}{(L/R)_{max}}\right)^m \exp\left[\frac{1}{\sigma}\left|\ln\left(\frac{(L/R)}{(L/R)_{max}}\right)\right|^n\right] \tag{8}$$

where

$$(L/R)/(L/R)_{max} < 1;\ m = -0.16,\ n = 1.61,\ \sigma = -1.86, \tag{9}$$

$$(L/R)/(L/R)_{max} > 1;\ m = -2.32,\ n = 0.889,\ \sigma = 0.494. \tag{10}$$

In completing the approximation, expressions for $(F_{\theta=90})_{max}$ and $(L/R)_{max}$ were developed from their variations shown by the points plotted in Fig. 5. The solid lines are curves computed according to the following equations:

$$(L/R)_{max} = 2.42(C/R) - 2.24, \tag{11}$$

$$\frac{(F_{\theta=90})_{max}}{(F_{\theta=90})_{max}|_{C/R=2}} = \left(\frac{(L/R)_{max}}{(L/R)_{max}|_{C/R=2}}\right)^{-0.95} \tag{12}$$

where, for the just-touching position ($C/R = 2$):

$$(F_{\theta=90})_{max}|_{C/R=2} = 0.178, \tag{13}$$

$$(L/R)_{max}|_{C/R=2} = 2.59. \tag{14}$$

Equations (11) and (12) represent the computed points to within 1.0% on the average. Combining equations (11)–(14),

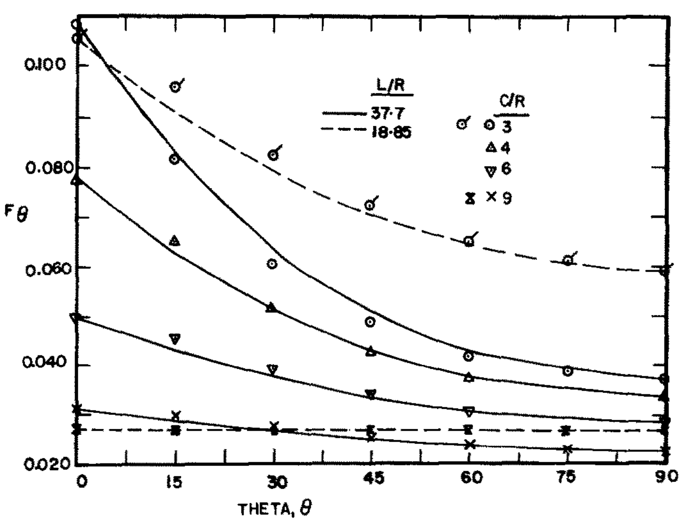

FIG. 2. Configuration factors for mid-point θ-rotations [Fig. 1(b)]. Data points: numerical integration; curves: equation (2).

an expression for $(F_{\theta=90})_{max}$ as a function (C/R) may be written as

$$(F_{\theta=90})_{max} = 0.205[1.08(C/R) - 1]^{-0.95}. \quad (15)$$

Equations (8)–(15) allow $F_{\theta=90}$ to be computed directly. The agreement between such computations and those obtained from numerical integration is shown in Fig. 4. For scaled lengths greater than 0.1, $F_{\theta=90}$ is predicted on the average to within 2.7% with a maximum difference of 6.0%.

With the above specification for $F_{\theta=90}$ plus the result for F_0 given by equations (3)–(7), F_θ may be calculated from equation (2). Configuration factors computed according to the above closed form result are compared to the results of numerical integration in Fig. 2. The average discrepancy for the cases shown is less than 2.5% with the largest difference being 6.4%. The agreement usually improves as the cylinder length decreases or the spacing increases since the difference between F_0 and $F_{\theta=90}$ becomes smaller under these conditions and hence the accuracy of the results is less sensitive to errors in the assumed interpolating formula.

End-point rotation—Fig. 1(c)

For two cylinders of equal length and diameter wherein one is rotated about its end-point, the configuration factor is symmetric with respect to $\theta = 180°$. As a result, the functional form used for mid-point rotations were initially chosen for this case too (with $F_{\theta=180}$ replacing $F_{\theta=90}$). This approach, however, was unsuccessful. Several other single-term expressions were also tried and finally the following equations for two separate angular domains were adopted:

$$0° \leq \theta \leq 90°, \quad \frac{F'_\theta}{F_0} = \left(\frac{F'_{\theta=90}}{F_0}\right)^{\theta/90} \quad (16)$$

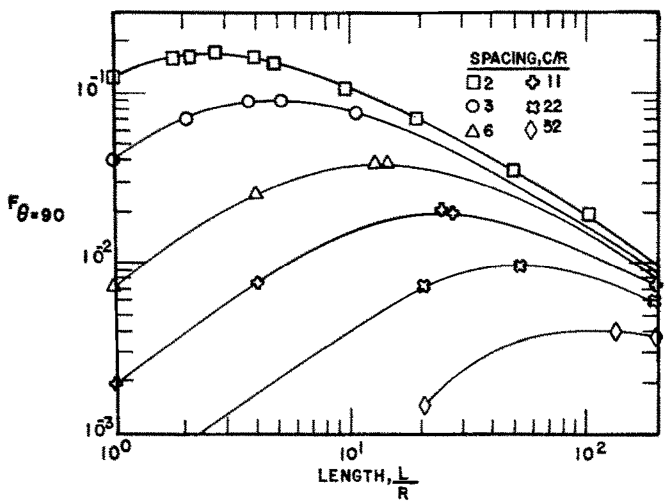

FIG. 3. Configuration factors for $\theta = 90°$. Data points: numerical integration; curves: lines drawn through the points.

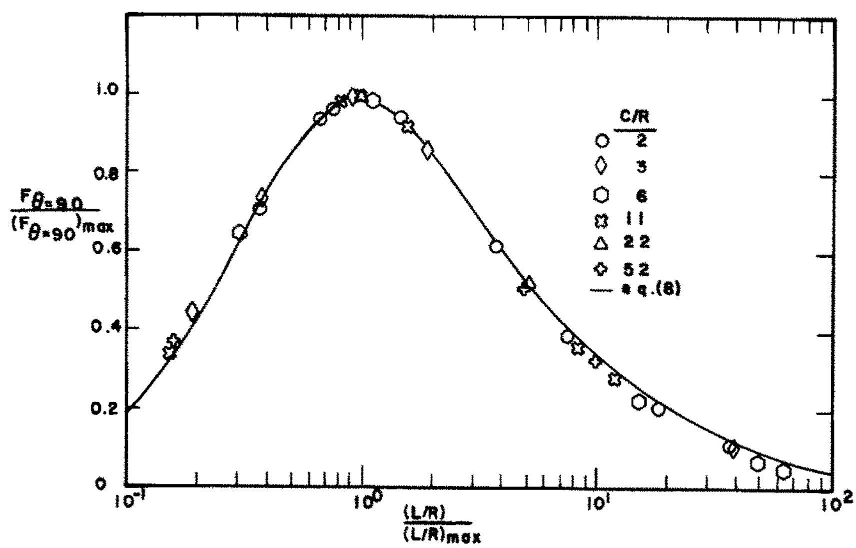

FIG. 4. Configuration factors for $\theta = 90°$ in scaled variables. Data points: numerical integration; curve: equation (8).

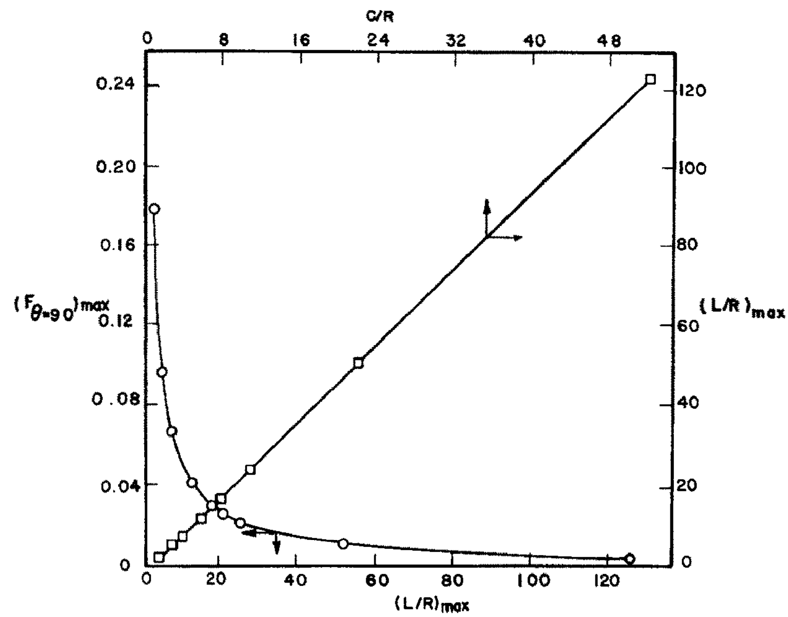

FIG. 5. Relationship between $(F_{\theta=90})_{\max}$ and $(L/R)_{\max}$; dependence of $(L/R)_{\max}$ on (C/R). Data points: numerical integration; curves: equations (11) and (12).

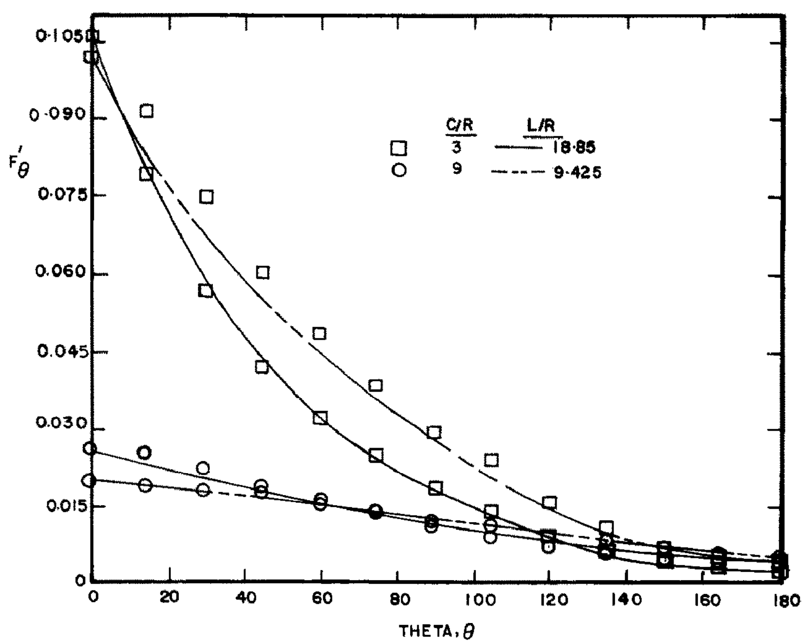

FIG. 6. Configuration factors for end-point θ-rotations. Data points: numerical integration; curves: equations (16) and (17).

$$90^\circ \le \theta \le 180^\circ,\quad \frac{F'_\theta}{F'_{\theta=90}} = \left(\frac{F'_{\theta=180}}{F'_{\theta=90}}\right)^{f(\theta)} \tag{17}$$

$$f(\theta) = 1.39\left[\tanh\left(\frac{\theta-90}{90}\right)\right]^{1.2}. \tag{18}$$

The above equations are exact at 0, 90 and 180°. The primed configuration factors (F') refer to end-point rotations. The unprimed refer to mid-point rotations: $F_{\theta=90}$ is given by equation (8) and F_0 by equation (3). The quantities $F'_{\theta=90}$ and $F'_{\theta=180}$ may be obtained from configuration factor algebra and are given by

$$F'_{\theta=90} = F_{\theta=90}/2 \tag{19}$$

$$F'_{\theta=180} = F_0|_{2L/R} - F_0|_{L/R} \tag{20}$$

In Fig. 6, values of F'_θ computed according to the above equations are compared to the results of numerical integration. Agreement to within 4.8% is obtained on the average with discrepancies near 11.0% occurring for short, closely spaced cylinders at angles of rotation between 20 and 45°.

ϕ-ROTATION

Configuration factors for half to whole length cylinders were investigated for pure ϕ-rotations [$\theta = 0°$, see Fig. 1(d)]. A typical variation is shown in Fig. 7. The results from numerical integration are given by the plotted points. The solid line was calculated from the following equation which is similar to equation (12) for pure θ-rotations:

$$\frac{F_\phi}{F_0} = \left(\frac{F_{\phi=90}}{F_0}\right)^{\sin\phi}. \tag{21}$$

In the above, F_0 is the configuration factor for half- to whole-length cylinders in the parallel orientation which, by configuration factor algebra, equals the configuration factor for two whole length cylinders in the parallel orientation. Therefore F_0 is given by equation (3) in which L corresponds to the full-length cylinder.

In determining $F_{\phi=90}$ the same approach was taken as for $F_{\theta=90}$. Figure 8 is a plot of $F_{\phi=90}$ as a function of spacing and cylinder length (analogous to Fig. 3 for $F_{\theta=90}$). Figure 9 shows how the points in Fig. 8 collapse when $F_{\phi=90}$ is scaled by $(F_{\phi=90})_{max}$ and $(L/2R)$ is scaled by $(L/2R)_{max}$, its value corresponding to $(F_{\phi=90})_{max}$. This scaling is seen to be

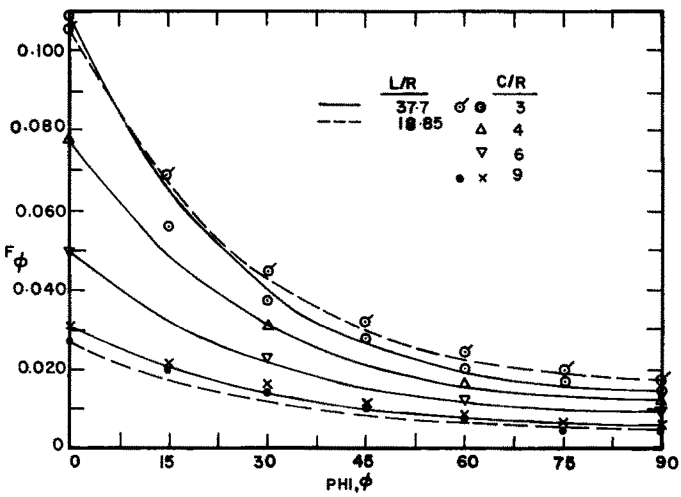

FIG. 7. Configuration factors for ϕ-rotations. Data points: numerical integration; curves: equation (21).

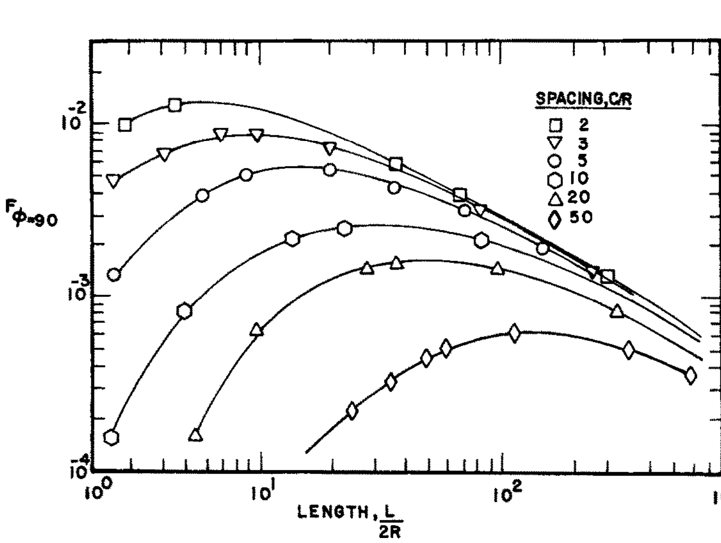

FIG. 8. Configuration factors for $\phi = 90°$. Data points: numerical integration; curves: lines drawn through the points.

appropriate for scaled lengths greater than 0.4. The solid line in Fig. 9 represents values computed according to the following probability distribution function:

$$\frac{F_{\phi=90}}{(F_{\phi=90})_{\max}} = \left(\frac{(L/2R)}{(L/R)_{\max}}\right)^{p} \exp\left[\frac{1}{\sigma'}\left|\ln\left[\frac{(L/2R)}{(L/2R)_{\max}}\right]\right|^{q}\right] \tag{22}$$

where

$$(L/2R)/(L/2R)_{\max} < 1;\ p = -0.0778,\ q = 1.93,\ \sigma' = -2.08, \tag{23}$$

$$(L/2R)/(L/2R)_{\max} > 1;\ p = 0.0579,\ q = 1.57,\ \sigma' = -3.46. \tag{24}$$

The agreement is seen to be excellent for scaled lengths greater than 0.4. At shorter lengths, good agreement is achieved only for spacings greater than 10. Overall, the average discrepancy is 4.4%.

The variations of $(L/2R)_{\max}$ and $(F_{\theta=90})_{\max}$ are shown in Fig. 10. The solid lines are the variations predicted by the following equations:

$$(L/2R)_{\max} = 3.1\,[(C/R) - 1]^{0.94} + 2.6, \tag{25}$$

$$\frac{(F_{\phi=90})_{\max}}{(F_{\phi=90})_{\max}|_{C/R=1}} = \left(\frac{(L/2R)_{\max}}{(L/2R)_{\max}|_{C/R=1}}\right)^{-0.95} \tag{26}$$

where, for the just-touching position ($C/R = 1$):

$$(F_{\phi=90})_{\max}|_{C/R=1} = 0.0257, \tag{27}$$

$$(L/2R)_{\max}|_{C/R=1} = 2.6. \tag{28}$$

Combining equations (25)–(28), an expression for $(F_{\phi=90})_{\max}$ as a function of (C/R) may be written:

$$(F_{\phi=90})_{\max} = 0.0257\{1.19[(C/R) - 1]^{0.94} + 1.0\}^{-0.95}. \tag{29}$$

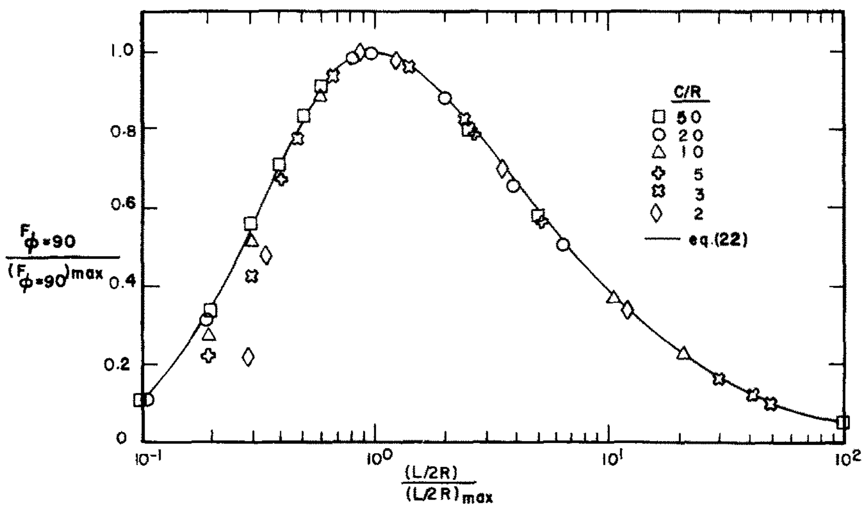

FIG. 9. Configuration factors for $\phi = 90°$ in scaled variables. Data points: numerical integration; curve: equation (22).

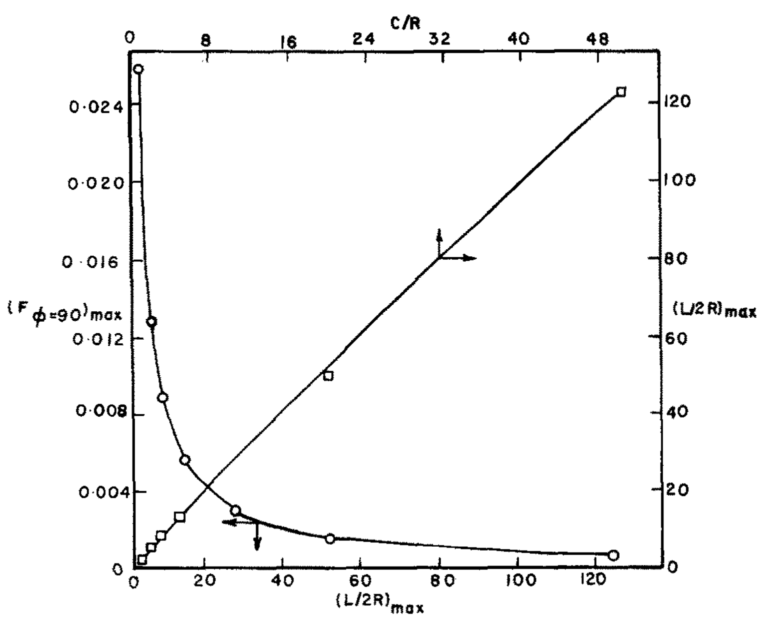

FIG. 10. Relationship between $(F_{\phi=90})_{\max}$ and $(L/2R)_{\max}$; dependence of $(L/2R)_{\max}$ upon (C/R). Data points: numerical integration; curves: equations (25) and (26).

In Fig. 7, the values of F_ϕ computed using the above equations are seen to compare favorably with the results of numerical integration. The average discrepancy for the cases shown is about 8% with the largest being 21%. Generally, the agreement is better at closer spacings.

COMBINED θ AND ϕ ROTATIONS

Arbitrary orientations of the two cylinders may be prescribed by specifying the distance between the cylinders plus the two angular rotations θ and ϕ. Again, the convention adopted in this study was to perform the ϕ-rotation first [see Fig. 1(e)]. Under these combined rotations, the configuration factors for whole-length to half-length cylinders were investigated. An approximate expression for determining $F(\phi, \theta)$ was developed [9] by defining a function which would satisfy the limiting conditions for various θ and ϕ combinations of 0 and 90°. The postulated function is

$$\frac{F(\phi,\theta)}{F(0,0)} = \left(\frac{F(\phi,90)}{F(\phi,0)}\right)^{\sin\theta}\left(\frac{F(90,\theta)}{F(0,0)}\right)^{\sin\phi} \tag{30}$$

where

$$F(0,0) = F_0, \text{equation (3)} \tag{31}$$

$$\left.\begin{aligned} F(90,\theta) &= F_{\phi=90} \quad (32)\\ F(\phi,90) &= F_{\phi=90} \quad (33)\end{aligned}\right\}\text{equation (21)}$$

$$F(\phi,0) = F_\phi, \text{equation (20)} \tag{34}$$

Combining equations (30)–(34) yield an expression for $F(\phi, \theta)$ in terms of previously defined functions:

$$\frac{F(\phi,\theta)}{F_0} = \left(\frac{F_{\phi=90}}{F_\phi}\right)^{\sin\theta}\left(\frac{F_{\phi=90}}{F_0}\right)^{\sin\phi}. \tag{35}$$

The above equation is intended to be used only when θ and ϕ both lie between 0 and 90° since $F(\phi, \theta)$ is generally not symmetric with respect to either $\theta = 90°$ or $\phi = 90°$. In Table 1 a comparison is given between the values predicted by equation (35) and the results of numerical integration. For the cases computed, the maximum discrepancy was about 30%. The largest errors occur when either or both of the angles is near 45°. The minimum errors occur at angular combinations of 0 and 90° since the interpolating function was formulated to be accurate for these orientations.

CONCLUSION

Numerical computations of configuration factors for obliquely oriented cylinders have been presented for a variety of cylinder spacings, lengths and angular orientations. Closed-form expressions have been developed which, in most cases, predict the configuration factors quite accurately. For each of the two distinct types of 90° orientations it was found that the configuration factors for a wide range of different spacings and lengths could be scaled to yield a single curve under most conditions. In addition, the cylinder lengths which yield a maximum configuration factor for a given spacing were also

Table 1. Configuration factors for whole to half-length cylinders for combined θ and ϕ-rotations

L/R	C/R	ϕ	θ	$100 \times F_{(L/R)-(L/2R)}$ Numerical integration	$100 \times F_{(L/R)-(L/2R)}$ equation (35)	L/R	C/R	ϕ	θ	$100 \times F_{(L/R)-(L/2R)}$ Numerical integration	$100 \times F_{(L/R)-(L/2R)}$ equation (35)
18.85	3	0	0	5.30	5.32	37.7	3	0	0	5.46	5.41
		0	90	2.99	2.96			0	90	1.88	1.92
		90	0	0.89	0.89			90	0	0.75	0.71
		45	0	1.66	1.83			45	0	1.33	1.27
		45	15	1.70	1.79			45	15	1.33	1.42
		45	30	1.81	2.10			45	30	1.35	1.57
		45	45	2.24	2.42			45	45	1.42	1.70
		45	60	2.25	2.70			45	60	1.52	1.82
		45	75	2.57	2.89			45	75	1.67	1.90
		45	90	2.99	2.96			45	90	1.88	1.92
		0	45	3.59	3.51			0	45	2.45	2.61
		15	45	2.96	3.06			15	45	2.07	2.23
		30	45	2.42	2.70			30	45	1.71	1.93
		60	45	1.68	2.23			60	45	1.21	1.55
		75	45	1.49	2.12			75	45	1.09	1.46
		90	30	1.13	1.62			90	30	0.88	1.17
		90	45	2.99	2.08			90	45	1.04	1.46
		90	60	1.84	2.52			90	60	1.25	1.68
18.85	9	0	0	1.36	1.36	37.7	9	0	0	1.57	1.56
		0	90	1.33	1.32			0	90	1.14	1.14
		90	0	0.23	0.29			90	0	0.31	0.30
		45	0	0.56	0.56			45	0	0.60	0.60
		45	15	0.59	0.60			45	15	0.62	0.71
		45	30	0.68	0.77			45	30	0.68	0.83
		45	45	0.80	0.96			45	45	0.77	0.95
		45	60	0.95	1.14			45	60	0.87	1.05
		45	75	1.12	1.27			45	75	0.99	1.12
		45	90	1.33	1.32			45	90	1.14	1.15
		0	45	1.34	1.34			0	45	1.29	1.25
		15	45	1.13	1.18			15	45	1.08	1.11
		30	45	0.95	1.06			30	45	0.90	0.99
		60	45	0.69	0.90			60	45	0.66	0.83
		75	45	0.62	0.86			75	45	0.60	0.79
		90	30	0.42	0.62			90	30	0.45	0.59
		90	60	0.80	1.07			90	60	0.74	0.96

determined for these orientations. Results for other cylinder orientations were presented for several conditions. The accuracy of the approximate expressions was found to be quite good for both pure θ and pure ϕ rotations. Combined rotations were not represented as accurately.

REFERENCES

1. J. A. Stevenson and J. C. Grafton, Radiation heat transfer analysis for space vehicles, N. Am. Aviat. Rep. SID-61-91, 1973–175 (1961).
2. E. M. Sparrow and V. K. Jonsson, Angle factors for radiant interchange between parallel-oriented tubes, *J. Heat Transfer* **85**, 382–384 (1963).
3. L. R. Glicksman, Approximations for configuration factors between cylinders, unpublished technical report, M. I. T., Sept. (1972).
4. H. C. Hottel and A. F. Sarofim, *Radiative Transfer*, p. 35. McGraw-Hill, New York (1967).
5. R. S. Dummer and W. T. Breckenridge, Jr., Radiation Configuration Factors Program, Rep. ERR-AN-224, General Dynamics/Astronautics, Feb. (1963).
6. Arthur D. Little, Inc., Program Manual for CONSHAD, ADL Ref. C-79393-01 (1976).
7. P. Moon, *The Scientific Basis of Illuminating Engineering* (revised edn.). Dover Publications, New York (1961).
8. E. M. Sparrow, A new and simpler formulation for radiative angle factors, *J. Heat Transfer* **85**, 81–88 (1963).
9. R. H. Spedden, Thermal radiation view factor analysis for finite circular cylinders, M.S. thesis, M. I. T., Aug. (1977).
10. A. Ameri, Radiation Configuration Factors for Obliquely Oriented Finite Length Circular Cylinders, M.S. thesis, State University of New York at Buffalo, October (1981).

Int. J. Heat Mass Transfer. Vol. 25, No. 5, pp. 736–739, 1982
Printed in Great Britain
0017-9310/82/050736-04 $03.00/0

ANALYTIC SOLUTION FOR THE EIGENVALUES AND COEFFICIENTS OF THE GRAETZ PROBLEM WITH THIRD KIND BOUNDARY CONDITION

M. N. Özişik and M. S. Sadeghipour
Mechanical and Aerospace Engineering Department,
North Carolina State University, Raleigh, NC 27650, U.S.A.

(*Received* 1 *June* 1981 *and in revised form* 19 *October* 1981)

NOMENCLATURE

$C_nR_n(1)$, coefficient used in equations (4) and (5);
H, $= hr_w/k$, Biot number;
h, heat transfer coefficient for external ambient;
h_z, heat transfer coefficient for flow inside the tube;
k, thermal conductivity of the fluid;
K, $= \lambda_n/4$;
Nu_z, $= 2r_wh_z/k$, Nusselt number;
Pr, $= \nu/\alpha$, Prandtl number;
r, $= r'/r_w$, dimensionless radial coordinate;
r', dimensional radial coordinate;
r_w, inside radius of the tube;
Re, $= 2r_wU_m/\nu$, Reynolds number;
T_0, T_∞, inlet and ambient temperatures respectively;
Um, mean velocity;
z, dimensionless axial coordinate, $2z'/r_wRePr$;
z', axial coordinate.

Greek symbols
θ, $=(T-T_\infty)/(T_0-T_\infty)$, dimensionless temperature;
λ_n, eigenvalue.

INTRODUCTION

The Graetz problem for laminar flow inside a circular tube subjected to the boundary condition of the third kind at the tube wall is encountered in numerous engineering applications and has been studied by few investigators [1, 2]. For the analysis of such problems, the local Nusselt number is a quantity of practical interest and its determination requires a knowledge of the eigenvalues and the eigenfunctions for the problem. Hsu [2] solved such an eigenvalue problem numerically and also presented some asymptotic expressions for the eigenvalues and the coefficients. Here we present highly accurate analytic expressions for the determination of the eigenvalues and the coefficients that are applicable over the entire range of the Biot number from zero to infinity.

ANALYSIS

We consider thermally developing laminar flow inside a circular tube with fully developed velocity profile and subjected to the boundary condition of the third kind at the tube wall. For a constant property, incompressible fluid with no heat generation and neglecting the viscous energy dissipation, the mathematical formulation of this heat transfer problem is given in the dimensionless form as

$$2(1-r^2)\frac{\partial\theta(r,z)}{\partial z} = \frac{1}{r}\frac{\partial}{\partial r}\left(r\frac{\partial\theta}{\partial r}\right), \quad 0 \le r \le 1, \quad z > 0 \tag{1a}$$

$$\frac{\partial\theta(0,z)}{\partial r} = 0, \quad z > 0 \tag{1b}$$

$$\frac{\partial\theta(1,z)}{\partial r} + H\theta(1,z) = 0, \quad z > 0 \tag{1c}$$

$$\theta(r,0) = 1, \quad 0 \le r \le 1. \tag{1d}$$

The solution of this heat transfer problem is given by

$$\theta(r,z) = \sum_{n=0}^{\infty} C_nR_n(r)e^{-\lambda_n^2 z/2} \tag{2}$$